SJER Scientific Journal of Engineering Research

futuristech PT. Teknologi Futuristik Indonesia

Received: March 24, 2026; Revised: June 12, 2026; Accepted: June 18, 2026; Published: June 21, 2026; Current version: June 21, 2026. e-ISSN: 3109-1725
Digital Object Identifier 10.64539/sjer.v2i4.2026.470

Article

Effect of Ni-Cr on the Mechanical properties, Machinability, Microstructure and Corrosion Behaviour of Al5Si3Cu Alloy

Omogbolade L. Adepitan[1,*], Olusegun Olufemi Ajide[2]

[1] Department of Mechanical Engineering, Lead City University, Ibadan 200255, Nigeria; e-mail: adepitan.omogbolade@lcu.edu.ng (O. L. Adepitan).
[2] Department of Mechanical Engineering, University of Ibadan, Ibadan, Nigeria; e-mail: omogboladea@gmail.com (O. O. Ajide).
* Correspondence Author

The authors received no financial support for the research, authorship, and/or publication of this article.

Abstract: This study was designed to explore the effects of varying amounts of Nickel (Ni) and Chromium (Cr) on the mechanical, microstructural, corrosion, and machining properties of Al5Si3Cu alloy. Samples were prepared using a sand-casting method with Ni-Cr additions ranging from 2g to 10g, and analysed using spectroscopy, mechanical testing (hardness, tensile, impact, and compression), machinability evaluation, and wear testing via pin-on-disc. The evolved microstructure was observed using X-ray Diffraction (XRD) and Scanning Electron Microscope (SEM), while corrosion resistance was investigated using potentiodynamic polarisation. The results revealed that Ni-Cr additions led to a complex balance of effects. While corrosion resistance improved at 8g Ni-Cr, mechanical strength and machinability declined due to the formation of brittle intermetallic compounds. Wear resistance was highest at 2g Ni-Cr but deteriorated with higher additions. At 10g Ni-Cr, corrosion resistance and overall performance declined due to oversaturation and microstructural defects. It was concluded that varying percentage of Ni-Cr has different effect on these properties of the ternary alloy. However, excessive alloying resulted in embrittlement and reduced performance. The findings emphasise the importance of precisely controlling Ni-Cr content in aluminium alloys to achieve a desirable balance of properties. Future research should focus on composition optimisation and understanding intermetallic behaviour.

Keywords: Aluminium alloy, Alloying elements, Potentiodynamic polarisation, Microstructure, Intermetallic compounds.

1. Introduction

Steel is being replaced by aluminium alloys in applications that require lower weight and less maintenance. In addition to having a high strength-to-weight ratio and being reasonably priced, structural materials also need to be considered. Aluminium alloys possess desirable properties like good workability, ductility, thermal conductivity, corrosion resistance, and thermal conductivity [1]-[3]. Because of its good formability and workability, it can be easily hammered, forged and drawn to any shape and size. Unlike other metallic alloys, aluminium and its alloys react with atmospheric oxygen when exposed to air to form a protective oxide coat to prevent further oxidation of the metal alloy. The protective coating produced by this alloy serves as a corrosion shield, thereby making it highly corrosion-resistant [3]. Aluminium alloys, particularly those in the 4xxx series, are commonly utilised in structural and transportation applications due to their excellent balance of strength, corrosion behaviour, weldability, machinability, and formability [4]-[6]. These age-hardenable alloys primarily derive their strength from the precipitation of metastable β″ (Mg_5Si_6) phases during artificial ageing [5]. Aluminium-based alloys, particularly Al-Si-Cu systems, have gained considerable attention in engineering applications due to their balanced combination of light weight, castability, and mechanical strength. The incorporation of selected alloying elements such as nickel (Ni), chromium (Cr), magnesium (Mg), and others can significantly influ-

ence the microstructural evolution and performance characteristics of these alloys. In the specific case of Al5Si3Cu alloy, such elemental additions are critical in refining the grain structure, enhancing mechanical properties like tensile strength and hardness, improving corrosion resistance, and modifying machinability [6]. These effects are largely attributed to the formation of secondary phases, intermetallic compounds, and the control of solidification pathways. Understanding how each element interacts within the alloy matrix is essential for optimising its performance for automotive, aerospace, and structural applications, where component reliability and processing efficiency are key considerations. However, their performance in real-world applications depends heavily on the intentional addition of alloying elements, which play a crucial role in tailoring their corrosion behaviour, machinability, mechanical performance, and microstructural evolution [6]. The performance of these alloys is significantly influenced by the addition of specific alloying elements, which modulate their corrosion behaviour, machinability, mechanical properties, and microstructural evolution.

The impact of alloying elements on Al-Mg-Si alloys is complex. Elements such as copper (Cu), manganese (Mn), chromium (Cr), iron (Fe), nickel (Ni), and zinc (Zn) can modify the precipitation sequence, grain structure, and intermetallic phase distribution when added in precise amounts [4]-[6]. For instance, adding Cu can significantly increase strength by creating additional strengthening phases; however, it may also reduce corrosion resistance because of galvanic coupling with the matrix. Mn and Cr, typically used as grain refiners, help manage recrystallisation and promote dispersoid formation, which enhances toughness and resistance to localised corrosion. Conversely, elements like Fe commonly found as an impurity create large intermetallic particles that negatively impact ductility and corrosion resistance, although they can improve machinability under specific conditions by aiding in chip fragmentation[5]. Machinability, which encompasses tool wear, surface finish, and chip formation, is influenced by alloy composition and the morphology of intermetallic phases. Elements like Fe and Mn form hard particles that assist in breaking chips but may accelerate tool wear [7]-[10]. Lead (Pb) and bismuth (Bi), though less commonly used due to environmental concerns, have also been employed to enhance machinability through the formation of low-melting-point phases that lubricate the cutting zone [8].

Another major property influenced by doping aluminium alloy with alloy elements is its chemical reactivity. The corrosion behaviour of Al-Mg-Si alloys is particularly sensitive to the type and distribution of second-phase particles and precipitates. Microstructural features such as grain boundaries, precipitate-free zones (PFZs), and the nature of precipitates (e.g., β″, β′, Q′, and θ′ phases) are strongly influenced by alloying content and thermal treatments [9]-[10]. These features dictate susceptibility to intergranular corrosion (IGC), pitting, and exfoliation. Mechanical properties such as impact, tensile strength, and compressive strength are directly impacted by the precipitation hardening response, which is altered by alloying. The introduction of Cr, Ni, or Ag can modify the nucleation and growth kinetics of strengthening precipitates, influencing the age-hardening potential [11]-[15]. Furthermore, microstructural refinement through grain boundary engineering, controlled recrystallisation, and dispersoid strengthening significantly boosts mechanical performance and reliability [13]. The microstructure of Al-Mg-Si alloys evolves during processing and is influenced by the alloying elements. The addition of elements like Nickel (Ni) and Chromium (Cr) can alter the precipitation sequence, leading to the formation of different intermetallic phases that impact the mechanical properties [16]-[18]. The presence of Mn can promote recrystallisation and grain refinement, leading to improved mechanical properties. Additionally, the cooling rate and heat treatment processes significantly affect the distribution and size of precipitates, thereby influencing the overall microstructure and, consequently, the properties of the alloy.

The corrosion behaviour, machinability, mechanical properties, and microstructural evolution of Al5Si3Cu alloys are significantly influenced by the selection and concentration of alloying elements. The corrosion resistance of Al5Si3Cu alloys is primarily determined by their microstructural characteristics, which are influenced by the presence of alloying elements [11]-[15]. For instance, the addition of rare earth elements like lanthanum (La) has been shown to enhance corrosion resistance by forming a La-rich surface shell on Mg_2Si particles, thereby mitigating localised corrosion and pitting in chloride environments [17]-[20]. Despite the extensive use of Al5Si3Cu alloys, there remains a lack of comprehensive studies that systematically investigate the combined effects of various alloying elements on the corrosion behaviour, machinability response, mechanical properties, and microstructural evolution of these alloys. Existing research often focuses on individual elements or isolated aspects, leading to a fragmented understanding. Moreover, the interactions between different alloying elements and their synergistic or antagonistic effects are not well elucidated. This knowledge gap hinders the rational design of Al5Si3Cu alloys tailored for specific applications. Therefore, there is a need to study these four vital properties holistically to balance the mechanical strength, corrosion resistance, machinability, and microstructural characteristics.

This study aims to evaluate the effects of alloying elements, particularly chromium and nickel, on the corrosion behaviour, machinability, mechanical properties, and microstructural evolution of Al5Si3Cu alloys. It involves

the comparative analysis of both pure and Ni-Cr–doped Al5Si3Cu alloys. The research is significant for its contribution to sustainable materials engineering, aligning with UN Sustainable Development Goals (SDGs 9, 12, and 13) by promoting industrial innovation, responsible consumption, and climate action. Through improving material efficiency and durability while reducing environmental impact, this study supports the development of more resource-efficient and low-carbon manufacturing systems, ultimately fostering innovation and sustainability in engineering and infrastructure.

This paper is structured in four different sections: the introduction section that provides a broad understanding of the general study and the aim of the study; the materials and methodology sections which provide the detailed experimentation and the analysis techniques; the results and discussion section which provides detailed scientific explanation of results with discussion; and the conclusion section with inferences and recommendations.

2. Materials and Methods

2.1. Aluminium, Nickel and Chromium composition

Aluminium metal was prepared for analysis using the Spectro analysis method. The aluminium alloy scraps used were collected from automotive scraps. This decision was made to demonstrate that aluminium waste (especially in the automobile industry) in the environment can be valorised into an applicable material for use in engineering industries.

2.2. Alloy Preparation

High-purity aluminium Al5Si3Cu was sourced from scrap in an automobile workshop in Ibadan, southwestern Nigeria. Pure analytical grades of Nickel powder and chromium metal, as shown in Figure 1 and 2, were from a chemical company. A sand-casting method was used to prepare each sample of pure aluminium metal and aluminium alloys. Clay sand moulds were prepared with the different patterns for the tensile strength, impact, scanning electron microscope (SEM), and other tests that were carried out on the samples. The sand mould cavities represent the shape of each sample to be used. Before melting, the pure aluminium samples were properly cleaned with acetone to remove any form of grease, oil, oxides or any other contaminants. The aluminium metal was then placed into the crucible, which was later placed inside the furnace to be heated to its melting point of about 660 °C. The crucible containing the melted aluminium was brought out from the furnace and poured immediately into the already prepared sand-cast cavity mould to form the shape of the mould cavity, as shown in Figure 3. The poured aluminium melt was left to solidify, and the sand-cast mould was destroyed to get the pure aluminium sample. The dimensions of the obtained samples are shown in Figure 4.

The same process was employed in the doping of the Al5Si3Cu with Nickel and Chromium. An amount of aluminium was weighed, added to the crucible and placed inside the furnace to be melted to its melting point. Also, the weighed Nickel and Chromium were placed in another furnace to be pre-heated to about 350 °C due to their high temperature. The pre-heated 2g of Nickel and Chromium were then transferred into the red molten liquid aluminium with proper stirring to achieve homogeneity, and were allowed to stay in the furnace for another 20-30 minutes before being taken out to be poured into the already prepared sand-cast mould cavity and left to solidify. After the alloy had solidified, the sand-cast mould was destroyed to be able to access the formed sample. The process was repeated for 4g, 6g, 8g and 10g of Nickel and 4g, 6g, 8g and 10g of Chromium, which were added to 92g, 88g, 84g and 80g of aluminium alloy, respectively. The samples were further machined to remove some unwanted material and also shaped to the required dimensions for easy analysis. Figure 5 shows a sample of the specimen after being properly shaped (machined).

2.3. Mechanical Testing

2.3.1. Brinell hardness tests

A provided sample was cut to get its specific length. After that, the sample was filed with a hand file to harden its surface. This was said to have been done properly, provided one could see the image of the teeth on the surface of the filed sample. It was later ground using a grinding machine, in which the surface was ground. After which, the sample was fixed into the tensiometer, where it was subjected to a compression load of 250 kg for about 15 seconds, after which the indented diameter was measured by an eyepiece. A conversion table was used to determine the Brinell hardness number of the material. The Brinell hardness (BHN), which is the pressure per unit surface area of the indentation in kg per square meter, is calculated as follows:

$$BHN = W/(\pi D/2)(D - \sqrt{(D\text{^}2) - d\text{^}2}) \quad (1)$$

Where,

- W is the load on the indenter, kg
- D is the diameter of the steel ball, mm
- d is the average measured diameter of the indentation, mm

2.3.2. Izod impact test

The impact phenomenon is very important in governing the life of a structure. An arm held at a specific height has constant potential energy. The arm struck this sample and broke it due to the energy absorbed; its impact strength is determined. The Izod impact differs from the Charpy impact test in that the sample is held in a cantile-

Figure 1. Pure sample of the Chromium stone.

Figure 2. Pure Sample of Nickel powder.

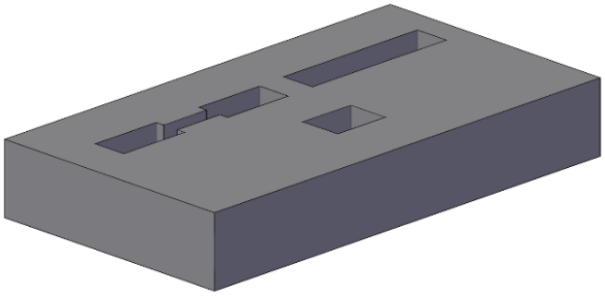

Figure 3. Sand-mould Cavities.

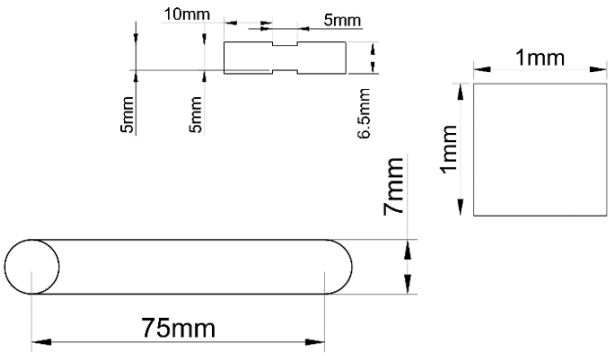

Figure 4. Dimensions of Samples.

ver beam configuration instead of the three-point bending configuration. This test can also be used to determine the notch sensitivity.

2.3.3. Tensile test

The tensile test is a fundamental mechanical test used to determine how materials behave under axial stretching loads. It provides key mechanical properties such a**s ultimate tensile strength (UTS), yield strength, elongation,** and **Young's modulus,** which are critical for assessing a material's structural performance. Tensile strength testing of all specimens was conducted as per ASTM 8 standard. Three identical test specimens for each section thickness per sample were tested at room temperature with a strain/ loading rate of 5 mm/min using a computerised Instron Testing Machine (model 3369). Load displacement plots were obtained on an X–Y recorder, and ultimate tensile strength, yield strength and percentage elongation values were calculated from these load displacement diagrams.

2.3.4. Compressive strength testing

Compressive strength testing of all specimens was conducted as per the ASTM standard. The accessories for the compressive test were fitted with the universal Instron machine. They were tested at room temperature with a strain/ loading rate of 5 mm/mn using a computerised Instron Testing Machine (model 3369). Load displacement plots were obtained on an X–Y recorder, and ultimate compressive strength, yield strength and percentage elongation values were calculated from these load displacement diagrams.

2.3.5. Wear test

The wear test was conducted using a pin-on-disc apparatus under dry wear conditions, following a systematic procedure. First, the initial weight of the specimen was recorded, after which the specimen was securely inserted and fixed into the specimen holder. A load was then applied to the supporting rod to ensure firm contact between the stylus pin and the specimen surface. The electric motor was switched on to rotate the specimen for 20 cycles, simulating wear under controlled conditions. Upon completion, the specimen was reweighed to determine material loss, and the sliding distance was measured to evaluate the extent of wear. The equation of wear below was used:

$$V = \frac{\Delta m}{\rho} \quad (1)$$

Where,

V is the wear volume

Δm is the change in mass

ρ is the density of the material

Figure 5. Samples of doped aluminium.

2.4. Machinability testing

This study was conducted on turning operations on unreinforced and Ni-Cr–reinforced Al5Si3Cu alloys to investigate Ni-Cr content and spindle speed on machinability. The reinforcement was varied by adding 0 g to 10 g of Ni-Cr in 2 g increments, and machining was performed at three spindle speeds: 400 rpm, 600 rpm, and 800 rpm. With standard carbide cutting tools, a conventional lathe machine was used under dry cutting conditions. Cutting force was measured using a dynamometer, while surface roughness (Ra) was evaluated using a surface profilometer after each pass. The experimental setup aimed to assess how Ni-Cr addition and speed variation influence tool-workpiece interaction, cutting resistance, and surface quality of the machined alloys.

2.5. Metallography

Visual examination suffices for macro-level analysis, but micro-examination requires aided techniques. The samples were therefore prepared for metallographic analysis through a three-stage process: grinding, polishing, and etching. Grinding involved using silicon carbide papers of increasing fineness (220 to 600 grit) under running water to achieve a flat, smooth surface and prevent overheating, with the sample rotated 90° between grit changes. Polishing was performed using a universal polishing machine with selvt-cloth and silicon carbide suspensions of 1 µm and 0.5 µm to attain a mirror-like finish. Etching, using 2g NITAL for ferrous and sodium hydroxide for non-ferrous materials, revealed the microstructure by selectively attacking grain boundaries. Final examination was conducted under an Accuscope metallurgical microscope at 400x and 800x magnifications.

2.6. X-ray Diffraction (XRD)

X-ray Diffraction (XRD) analysis was conducted using the Zeiss SmartEDS, X-ray Diffractometer to evaluate the phase composition of the fabricated composites. The equipment operated with a copper Kα radiation source at a wavelength of 1.5406 Å. The working voltage and current were set at 40 kV and 30 mA, respectively. Scanning was carried out within a 2θ range of 10° to 90°, using a step size of 0.02° and a scan speed of 2° per minute.

2.7. Scanned Electron Microscope (SEM)

Samples for SEM analysis must be appropriately sized and mounted on a specimen stub. Larger SEM models can accommodate and tilt 6-inch wafers for comprehensive examination. To enhance conductivity, samples are coated with platinum using sputter coating or evaporation methods. Environmental SEM (ESEM) allows for imaging in high-pressure conditions, neutralising surface charge and enhancing signal quality. For advanced imaging or X-ray microanalysis, samples may be embedded in resin and polished to a mirror finish.

2.8. Potentiodynamic Polarisation (PDP)

Potentiodynamic Polarisation (PDP) curve was performed in a three-electrode system using computer-controlled potentiostat/galvanostat (Autolab 302N) software. Platinum electrode was used as the counter electrode (CE), Ag/AgCl in 3M KCl electrolyte as the reference electrode (RE) while the sample served as the working electrode (WE). The area of the WE exposed to the medium was approximately 1 cm^2 for approximately 30 minutes. The sequential techniques were used for the analysis when the medium was allowed to attain a stable state at a steady open circuit potential without the flow of current.

3. Results and discussion

3.1. Elemental Compositions

The elemental composition results reveal distinct variations among the three samples, Aluminium, Chromium, and Nickel, reflecting their unique metallurgical characteristics and potential influence on alloy performance. Table 1 shows the summary of the elemental composition of the two alloying elements, as well as the pure Al5Si3Cu alloy. The aluminium sample contains a high Al content (92.90g), with significant Si (12.91g) and moderate Cu (3.62g), suggesting a typical Al5Si3Cu casting alloy suitable for improved fluidity and moderate strength applications. Conversely, the nickel sample exhibits a very high Ni content (54.2g) with substantial Fe (45.5g) and Mo (0.954g), which is typical of nickel-based super alloys designed for high-temperature strength and oxidation resistance. Trace elements such as Nb (0.094g) in the Ni sample could enhance creep resistance, while minor Ti (0.14g) in the Cr sample may aid grain refinement. The low levels of P and S across all samples indicate good metallurgical quality, minimising the risk of embrittlement.

3.2. Mechanical Test

3.2.1. Brinell hardness tests

Table 2 and Figure 6 show that the introduction of Nickel and Chromium significantly affects the Brinell

Table 1. Elemental Compositions.

Elements	Al	C	Co	Ca	Cr	Cu	Fe	Mg	Mn	Mo	N	Nb	Ni	P	S	Si	Ti	Sn	V	Zn
Aluminium	88.92 gw	-	-	-	0.034 gw	3.52 gw	0.61 gw	-	0.186 gw	-	-	-	0.06 gw	-	-	5.91 gw	-	-	-	0.76 gw
Chromium	-		1.17 gw	0.60 gw	88.17 gw	-	4.74 gw	-	0.90 gw	-	1.99 gw	-	1.12 gw	0.03 gw	0.024 gw	0.99 gw	0.14 gw	-	0.12 gw	0.006 gw
Nickel	0.021 gw	0.028 gw	-	-	0.006 gw	0.002 gw	24.479 gw	-	0.009 gw	0.954 gw	0.002 gw	0.094 gw	74.2 gw	0.11 gw	0.045 gw	0.001 gw	-	0.001 gw	0.048 gw	-

Table 2. Effect of varying Ni-Cr on BHN of Al5Si3Cu.

	Amount of Alloying Elements		Brinell's Hardness Number (BHN)			
	Chromium (g)	Nickel (g)	Sample 1	Sample 2	Sample 3	Sample average
1	0	0	93.03	87.67	85.56	88.75
2	2	2	60.02	82.57	67.50	70.03
3	4	4	80.90	60.71	72.10	71.24
4	6	6	74.95	56.71	69.42	67.03
5	8	8	46.11	56.72	57.47	53.43
6	10	10	67.50	60.42	67.58	65.17

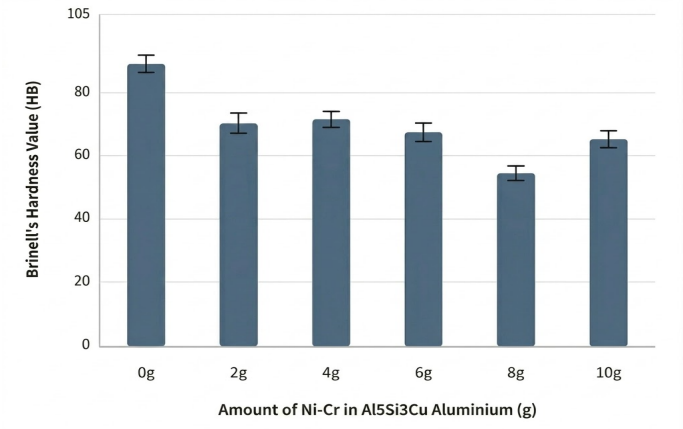

Figure 6. Brinell hardness values (HB) of Al5Si3Cu aluminium alloy reinforced with Ni-Cr (0–10 g). Error bars represent ± one standard deviation from triplicate measurements (n = 3).

hardness value (HB). The hardness of the Al5Si3Cu-Ni-Cr alloy dropped, with the highest hardness value among the Ni-Cr reinforced alloys obtained at 4 g of Ni-Cr. According to [21], the phase formation of Al_3Ni and δ-Al_3CuNi increases the coarseness of the Al5Si3Cu-Ni-Cr, which results in a drop in the microhardness. The connection between the coarse intermetallic particles reduces the hardness by acting as a fracture initiation site and hindering the effective load sharing across the alloy matrix. In 2024, a report by [22], on Al–15Si–4Ni–2Cu alloys shows that while Ni-rich intermetallics increase the hardness under quick solidification, slower cooling rates increase the coarsening as well as the microstructural separation, which undermines hardness gains. Moreover, the Al matrix does not support the solubility of Ni and Cr, and this could affect an important mechanism that supports the increase in hardness through lattice distortion. Instead, their tendency to precipitate as discrete compounds limits beneficial lattice strain effects. Furthermore, a Similar result was confirmed by [10], [23], that in spray-cast Al5Si-Cu-Ni alloys, the hardness peaked at intermediate Ni levels (around 2g) but declined at higher Ni content due to the excessive presence of brittle ε-Al_3Ni intermetallics that offered poor mechanical compatibility and localised strain rigidity. Therefore, while modest Ni-Cr additions reinforce high-temperature stability, their excess or improper distribution during casting and ageing can compromise hardness.

3.2.2. Impact Strength

From the obtained results section, specifically Table 3 and Figure 7, the addition of nickel (Ni) and chromium (Cr) to cast Al-5Si-3Cu alloys caused a precipitation of different intermetallic compounds such as Al_3Ni, Al_3CuNi, and Cr-rich phases, especially during ageing treatments. The

Table 3. Influence of varying Ni-Cr compositions on the impact strength of Al5Si3Cu.

	Amount of Alloying elements		Impact Value (Joules)			
	Chromium (g)	**Nickel (g)**	**Sample 1**	**Sample 2**	**Sample 3**	**Sample average**
1	0	0	17.52	17.16	17.43	17.37
2	2	2	13.18	13.20	13.22	13.20
3	4	4	14.12	14.32	14.26	14.23
4	6	6	15.52	15.72	15.62	15.62
5	8	8	14.84	14.68	14.78	14.77
6	10	10	14.16	14.42	14.32	14.30

Table 4. Influence of varying Ni-Cr on the tensile strength of Al5Si3Cu.

	Amount of Alloying Elements		Maximum Tensile Stress (MPa)			
	Chromium (g)	**Nickel (g)**	**Sample 1**	**Sample 2**	**Sample 3**	**Sample average**
1	0	0	92.48	82.28	87.38	87.38
2	2	2	38.59	46.03	42.32	42.31
3	4	4	69.36	69.32	72.77	72.73
4	6	6	64.58	44.05	54.30	54.31
5	8	8	77.00	75.49	76.19	76.24
6	10	10	42.28	89.39	64.98	57.41

Table 5. Shows the results with varying Ni-Cr additions on the tensile strain values.

	Amount of Alloying Elements		Maximum Tensile Strain × 10^{-4} (mm/mm)			
	Chromium (g)	**Nickel (g)**	**Sample 1**	**Sample 2**	**Sample 3**	**Sample average**
1	0	0	107	108	109	108
2	2	2	64	66	65	65
3	4	4	95	96	94	96
4	6	6	52	58	54	55
5	8	8	69	68	70	69
6	10	10	74	74	70	74

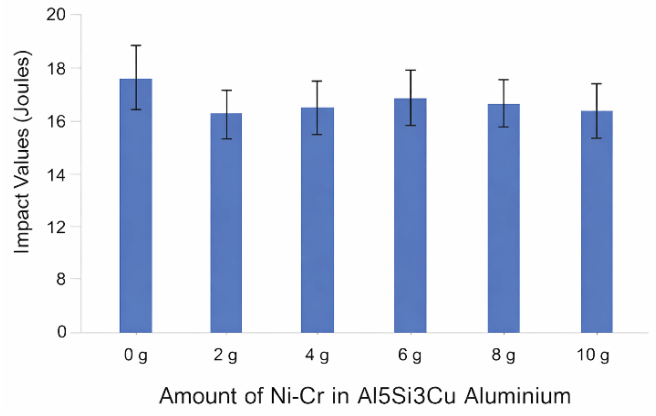

Figure 7. Impact value of Al5Si3Cu aluminium alloy reinforced with Ni-Cr (0–10 g). Error bars represent ± one standard deviation from triplicate measurements ($n = 3$).

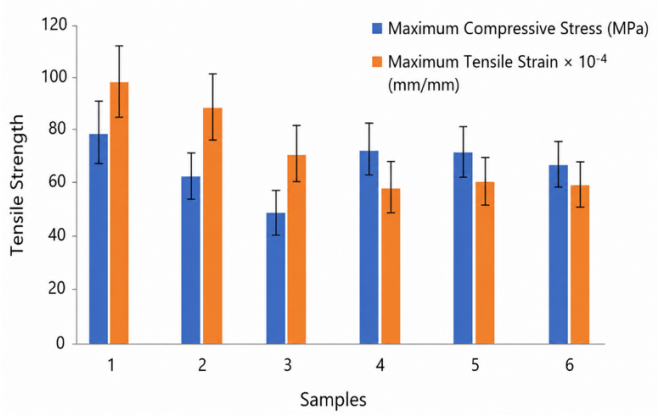

Figure 8. Stress-Strain relation of Al5Si3Cu aluminium alloy reinforced with Ni-Cr (0–10 g). Error bars represent ± one standard deviation from triplicate measurements ($n = 3$)

coarsening of this alloy during treatment produced interconnected brittle networks. These networks act as a source of crack initiation during impact loading. This hinders the alloy's ability to absorb fracture energy, thereby resulting in a sharp decline in impact toughness relative to the addition of a Ni-Cr-free base alloy. Furthermore, as discussed earlier, Ni and Cr exhibit **low solubility** in the α-Al matrix; for instance, **Al-3CuNi** formation consumes Cu needed for precipitation strengthening. A similar report was given by [24] in 2018**,** that higher Ni levels in 354-type alloys precipitate more brittle Ni-rich intermetallics, which operate as **stress concentrators** and cause early crack coalescence under impact loading. The changes in microstructural shift of the alloy's fracture behaviour from ductile to semi-brittle significantly reduce resilience to impact forces.

Table 6. Effect of varying Ni-Cr on Compressive Strength of Al5Si3Cu.

	Amount of Alloying Elements		Maximum Compressive Stress (MPa)			
	Chromium (g)	Nickel (g)	Sample 1	Sample 2	Sample 3	Sample average
1	0	0	60.04	60.00	60.00	60.02
2	2	2	45.12	45.13	45.10	45.12
3	4	4	53.09	51.08	52.07	52.09
4	6	6	47.06	47.05	47.05	47.07
5	8	8	28.90	30.00	29.85	29.95
6	10	10	40.05	39.89	39.80	39.85

Table 7. Effect of varying Ni-Cr on Compressive Strain of Al5Si3Cu.

	Amount of Alloying Elements		Maximum Tensile Strain × 10^{-4} (mm/mm)			
	Chromium (g)	Nickel (g)	Sample 1	Sample 2	Sample 3	Sample average
1	0	0	4.82	4.81	4.83	4.82
2	2	2	3.06	3.09	3.03	3.06
3	4	4	3.14	3.15	3.16	3.15
4	6	6	3.16	3.15	3.14	3.15
5	8	8	4.26	4.28	4.21	4.25
6	10	10	4.45	4.50	4.50	4.48

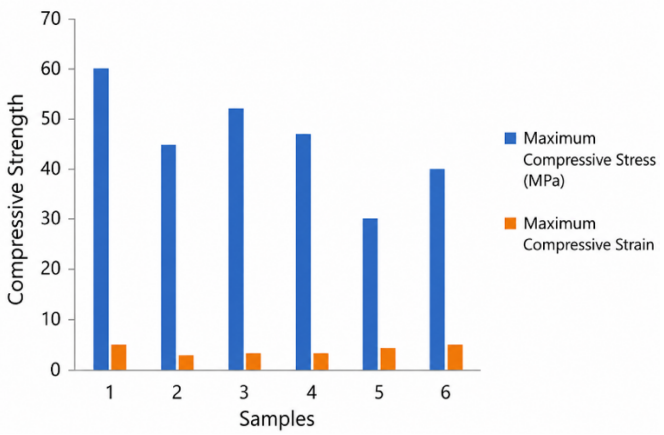

Figure 9. Effect of varying Ni-Cr on Compressive Strain of Al5Si3Cu.

3.2.3. Tensile Strength

From the results obtained in Tables 4 and 5, the introduction of Ni-Cr in varying weights (grams) decreases the tensile stresses and tensile strain of Al5Si3Cu when compared with the pure alloy, as shown in Figure 8. This could be due to the interaction between the precipitating Aluminium compounds of Ni and Cr, such as Al_9Cr_2 and Al_3Ni, during solidification. These compounds make the resulting alloy brittle and hard, thereby increasing wear resistance and poor interactions between the α-Al matrix, resulting in early cracks under tensile stress. Similar results were obtained in a study by [6] in 2023, where Ni-Cr were used to modify Al-Si-Cu alloys, which showed dependence on cooling rate and morphology of the particles. Likewise, a study conducted by [25] in 2022 using high-pressure torsion in the development of ultrafine grains of Al5Si3Cu alloys showed improved tensile strength and heavy dislocation structures. Furthermore, there is a weak cohesion force between grains due to the separation of chromium atoms during solidification. Therefore, under tensile loading, this can result in premature cracks (fractures) leading to a reduction in tensile strength and ductility of the alloy materials. The hard, non-deformable metallic compounds in the alloy increase the micro-cracks, and this can be seen from the mechanical properties, where 2 – 10g introduction of Ni-Cr modifies the mechanical properties of Al5Si3Cu, which results in the overall low tensile strength compared to unmodified Al5Si3Cu.

3.2.4. Compressive Strength

From the results obtained in Tables 6 and 7, the introduction of Ni-Cr in varying percentages has a significant effect on both the compressive stress and the compressive strain of the reinforced Al5Si3Cu compared to the unreinforced Al5Si3Cu, as shown in Figure 9. This could be caused by the lack of interaction between the formations of insoluble or heterogeneous compounds within the α-Al matrix that precipitated with the aluminium compounds of Ni and Cr, such as Al_9Cr_2 and Al_3Ni, during solidification. Similar results were obtained in a study by [6] in 2023, where Ni–Cr were used to modify Al5Si3Cu alloys, which showed dependence on cooling rate and morphology of the particles. Likewise, a study conducted by [25] in 2022, using high-pressure torsion in the development of ultrafine grains of Al5Si3Cu alloys, showed improved compressive strength and heavy dislocation structures. Furthermore, at 4g of Ni-Cr, the reinforced Al5Si3Cu demonstrated relatively high compressive stress compared to other Al5Si3Cu alloys. This could be caused by a reabsorption of Ni-Cr, giving room for a proper and seemingly homogeneous compounds formation within the structure; however, at Ni-Cr > 4g, the Al matrix has been saturated, and a weak cohesion force starts generating between grains due to grains' separation of excess chromium and Nickel atoms during solidification. Therefore, under compressive loading, this can result in premature cracks (fractures) leading to a reduction in com-

Table 8. Abrasive and wear data of Al5Si3Cu at varying Ni-Cr.

Samples	Initial Weight (g)	Final Weight (g)	Weight Loss (g)	Sliding Distance (mm)	Volume (ml)	Density (g/ml)	Volume Loss (mm^3)	Specific Wear Rate (mm^3/nm)	Wear Resistance (mm/nm^3)
0g	2.9758	2.9753	0.0005	1.42	1	2.9758	0.1680	0.0118	8.4524
2g	5.4006	5.4002	0.0004	2.74	2	2.7003	0.1481	0.0054	18.5010
4g	5.1331	5.1323	0.0008	2.69	2	2.5666	0.3117	0.0116	8.6301
6g	3.8743	3.8731	0.0012	2.59	1	3.8743	0.3097	0.0120	8.3629
8g	4.5203	4.5193	0.0010	2.65	1.5	3.0135	0.3318	0.0118	7.9867
10g	4.0899	4.0884	0.0015	2.83	1	4.0899	0.3668	0.0130	7.7154

pressive strength of the alloy materials. As discussed in the tensile stress, the hard, non-deformable metallic compounds in the alloy increase the micro-cracks, and this can be seen from the mechanical properties, where 2 g to 10 g introduction of Ni-Cr modifies the mechanical properties of Al5Si3Cu, resulting in the overall low compressive strength compared to unmodified Al5Si3Cu.

3.2.5. Wear Test

From the results in Table 8, the introduction of Ni and Cr additions to Al5Si3Cu had a significant impact on wear performance and, by implication, on the mechanical integrity of the alloy. The unreinforced sample of Al5Si3Cu showed a loss in volume of 0.1680 mm^3 and a specific wear rate of 0.0118 mm^3/Nm, which means the alloy is moderately resistant to abrasive forces with a corresponding wear resistance value of 8.4524 mm/mm^3. However, with the addition of 2g Ni-Cr to Al5Si3Cu, there was a noticeable improvement, as the volume loss reduced to 0.1481 mm^3, and the specific wear rate dropped to 0.0054 mm^3/Nm, representing the lowest wear rate across all compositions. This was due to negligible compound precipitation and intermetallic phases such as Al_3Ni and Cr-rich precipitates, which strengthen the matrix and improve hardness. Although the incorporation of Ni–Cr reinforcement resulted in a reduction in bulk hardness compared with the unreinforced alloy, the wear resistance was improved due to the presence of Ni–Cr intermetallic phases. Consequently, the 2g Ni-Cr sample demonstrated the highest wear resistance (18.5010 mm/mm^3), indicating optimum reinforcement at this composition level as reported by [26], [27]. However, further additions beyond 2g Ni-Cr led to a gradual decline in wear resistance. The 4g, 6g, 8g, and 10g of Ni-Cr samples displayed increasing volume losses and specific wear rates, with the 10g Ni-Cr sample recording the highest volume loss (0.3668 mm^3) and the lowest wear resistance (7.7154 mm/mm^3). As Ni-Cr additions increase beyond the optimal range, intermetallic phases grow larger and begin to coalesce, leading to a more brittle microstructure. In similar NiAl-Cr systems, the interface between the hard intermetallic and softer matrix becomes prone to intergranular cracking and delamination under sliding loads. These microstructural weaknesses manifest as increased volume loss and specific wear rate in samples with ≥ 4g Ni–Cr. The 10g Ni-Cr variant, showing the highest volume loss and lowest wear resistance, illustrates how excessive brittle phases decrease fracture toughness and facilitate crack propagation under abrasive stress.

3.3. Machining

Table 9 reveals a clear trend of increasing cutting force and surface roughness of the machining of both unreinforced and reinforced Al5Si3Cu with Ni-Cr. At 400 rpm, cutting force rose from 140 N to 190 N as Cr increased from 0 g to 10 g, while surface roughness (Ra) also increased from 3.20 µm to 3.85 µm. This result can be attributed to the formation of hard intermetallic compounds or carbides and solid solution strengthening caused by Cr, which increases the alloy's resistance to deformation during machining, as shown in both Figures 10 and 11. Ni-Cr alloys also exhibit rapid work-hardening, making chip removal more difficult and increasing tool material interaction, leading to higher forces and degraded surface quality as reported by [27]. The increase in Ra at lower speeds is linked to the higher likelihood of built-up edge formation and abrasive wear due to elevated cutting forces, which damage the tool and degrade surface finish. Increasing spindle speed from 400 rpm to 800 rpm consistently reduced both cutting force and surface roughness across all Cr compositions. For example, at 0 g Ni-Cr, the cutting force dropped from 140 N to 122 N, and Ra improved from 3.20 µm to 2.20 µm. This improvement can be attributed to the thermal softening at higher speeds of the intermetallic compounds rich in Ni-Cr, thereby reducing the cutting resistance and built-up edge formation. However, at 10 g Ni-Cr and 800 rpm, the cutting force remained relatively high at 160 N, and surface roughness increased to 3.00 µm, showing that more compounds rich in Ni-Cr are formed and thereby elevated thermal and mechanical stress conditions. The formation of Ni-Cr compounds' strain-hardening response remains strong even at higher temperatures, limiting the softening benefits typically gained from higher speeds, as reported by [27], [28].

3.4. XRD

The X-ray Diffraction (XRD) spectra show the precipitations in the alloy, with Figure 12a showing the spectrum for the pure Al5Si3Cu alloy. The spectrum showed no precipitation of any compound. The apparent absence of

Table 9. Machining Results for Al5Si3Cu with Varying Ni-Cr Additions at Different Cutting Speeds.

Ni-Cr (g)	Cutting Force (N)			Surface Roughness (Ra, μm)		
	400 rpm	600rpm	800 rpm	400 rpm	600rpm	800 rpm
0	140	130	122	3.20	2.75	2.20
2	155	145	132	3.30	2.85	2.40
4	165	152	140	3.45	3.05	2.55
6	175	162	150	3.65	3.15	2.70
8	185	174	161	3.75	3.25	2.65
10	190	175	160	3.85	3.40	3.00

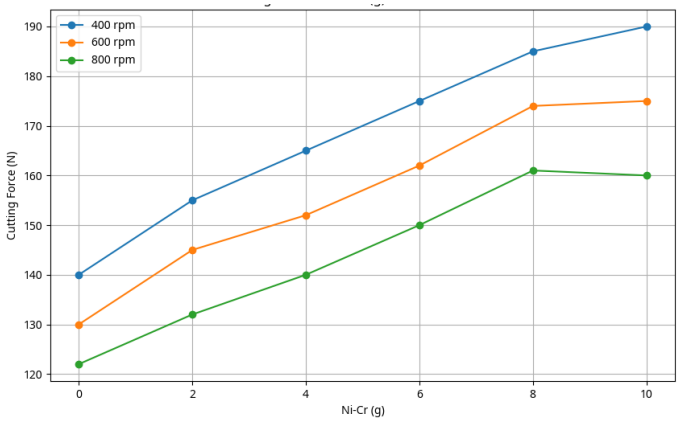

Figure 10. Cutting force vs. percentage of Ni-Cr in Al5Si3Cu.

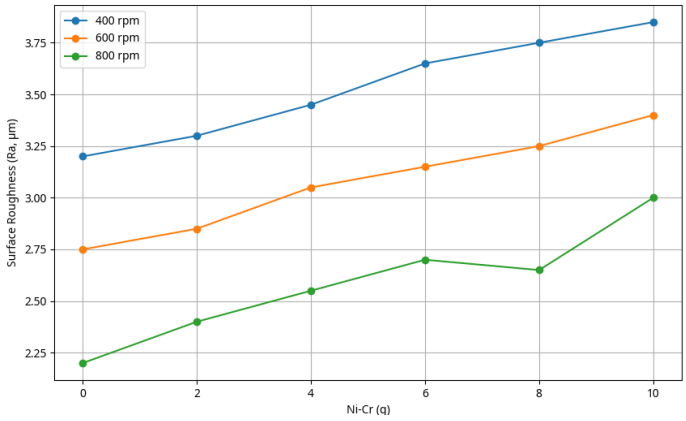

Figure 11. Surface Roughness vs. percentage of Ni-Cr in Al5Si3Cu.

secondary Ni–Cr phases in the XRD patterns of the 2 g and 4 g reinforced composites, as shown in Figure 12, despite their observation in SEM micrographs, can be attributed to the inherent detection limits of XRD. Phases present in very small volume fractions, as finely dispersed precipitates, or as localised clusters may not produce diffraction peaks with sufficient intensity to be distinguished from the matrix background. SEM, on the other hand, provides localised microstructural information and is capable of detecting such dispersed or clustered features. Therefore, the Ni–Cr dispersoids observed in SEM at lower reinforcement levels are likely below the detection threshold of XRD rather than being absent from the microstructure. This highlights the complementary roles of XRD and SEM in characterising phase evolution within the developed composites. This could be caused by the absorption of the Ni-Cr elements, leading to a **supersaturated solid solution,** without sufficient driving force for intermetallic nucleation. According to the results obtained by [29] in 2023, low Ni content (below ~1 g) results in minimal Ni-rich precipitates and retains mechanical properties through solid-solution effects rather than precipitated reinforcement. In the XRD results by **Cao's analysis, there is a diminishing Ni Al peak with reducing Ni,** aligning with our findings at 4 g Ni- Cr, where XRD indicates no secondary phase formation. However, at 6 g, 8 g, and 10g of Ni-Cr in Al5Si3Cu alloys, their **low solubility in the *α*-Al matrix** enhances the formation of **distinct intermetallic precipitates,** as confirmed by XRD peaks corresponding to Ni-Al and Cr-rich phases as shown in Figure 12d, e and f. Similar results were reported by **Cao *et al.* (2023)** in the investigation of Al-Si-Cu-Mg alloys with varying Ni content; the reports show that higher Ni promotes coarse, brittle Ni-rich intermetallics that manifest clearly in XRD patterns. Additionally, results obtained by [30] in 2024 demonstrated in Cu-Ni-Si-Cr systems that Cr suppresses undesirable phase coarsening but, when combined with high Ni, encourages heterogeneous nucleation of Ni_2Cr or NiAl phases, detectable using both XRD and TEM. Furthermore, the precipitation threshold lies between 4g and 10g Ni-Cr, below which the alloy remains homogeneous and beyond which discrete intermetallic phases form, affecting mechanical and thermal behaviour.

3.5. SEM

The SEM image of pure Al5Si3Cu shows a consistent microstructure of *α*-Al matrix with dispersed Al_2Cu and Si-rich phases and an absence of a secondary phase, suggesting a high level of homogeneity, as reported by [30], [31]. The image shown in Figure 13b contains 2g Ni-Cr with early-stage grain refinement and growth inhibition due to Ni-Cr. Figure 13c and Figure 13e show a more pronounced Ni-Cr forming localised clusters, which conform to the findings of [32]. In which the introduction of Ni-Cr leads to discontinuous intermetallic networks. Figure 13d shows well-distributed and uniform Ni-Cr with an intermetallic phase forming along the boundary. Finally, Figure 13f shows the 10g Ni-Cr with a dense reinforcing network phase, which significantly altered the alloy's mechanical behaviour. A report by [33] in 2023 indicates that Ni-Cr ≥ 10g induces precipitation hardening, but an excessive amount may lead to reduced ductility due to brittle intermetallic formation. Table 10

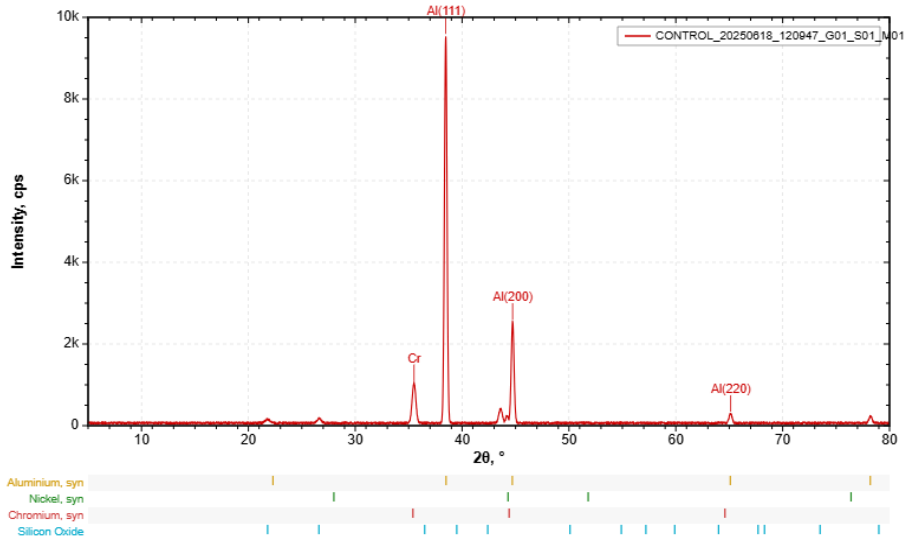
Al(111)
CONTROL_20250618_120947_G01_S01_M01
Intensity, cps
Cr
Al(200)
Al(220)
2θ, °
Aluminium, syn
Nickel, syn
Chromium, syn
Silicon Oxide

(a)

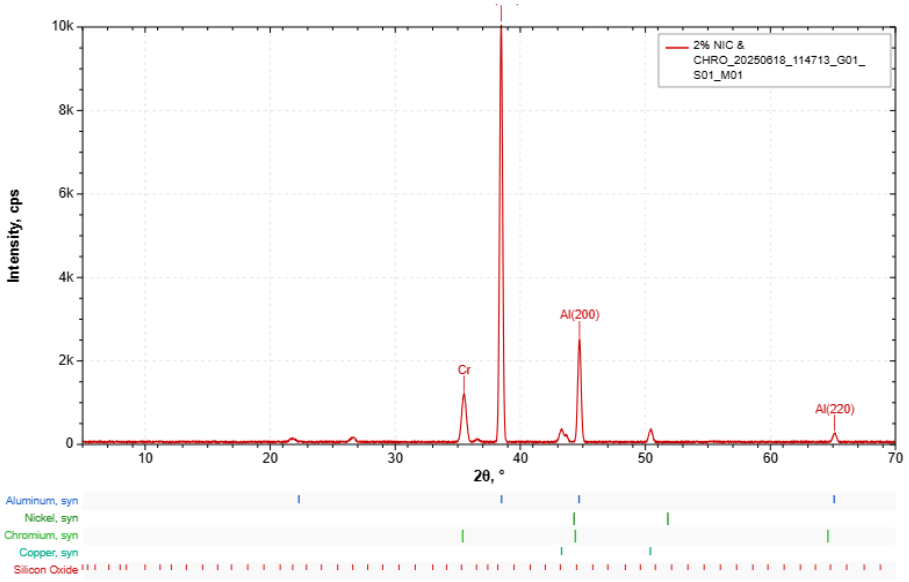
2% NIC & CHRO_20250618_114713_G01_S01_M01
Intensity, cps
Cr
Al(200)
Al(220)
2θ, °
Aluminum, syn
Nickel, syn
Chromium, syn
Copper, syn
Silicon Oxide

(b)

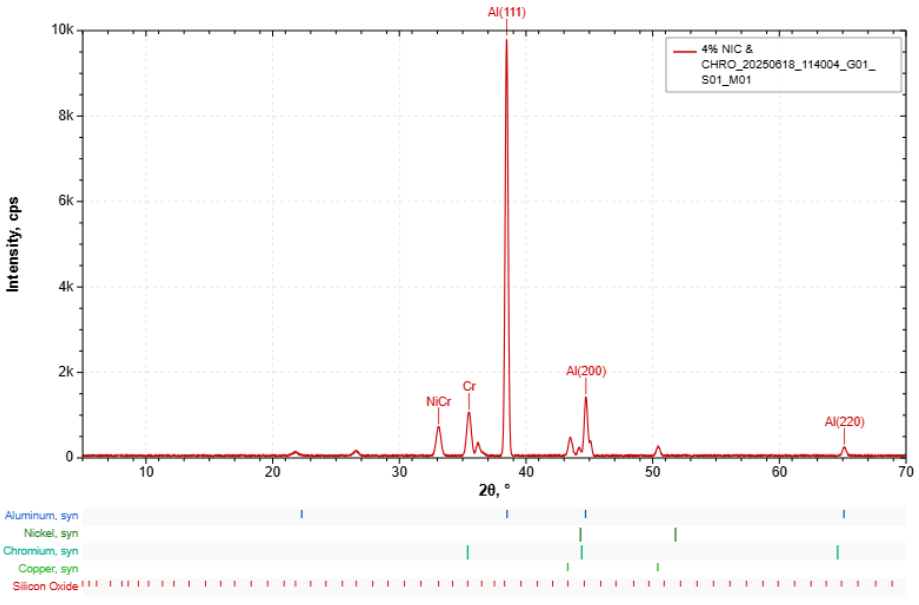
Al(111)
4% NIC & CHRO_20250618_114004_G01_S01_M01
Intensity, cps
NiCr
Cr
Al(200)
Al(220)
2θ, °
Aluminum, syn
Nickel, syn
Chromium, syn
Copper, syn
Silicon Oxide

(c)

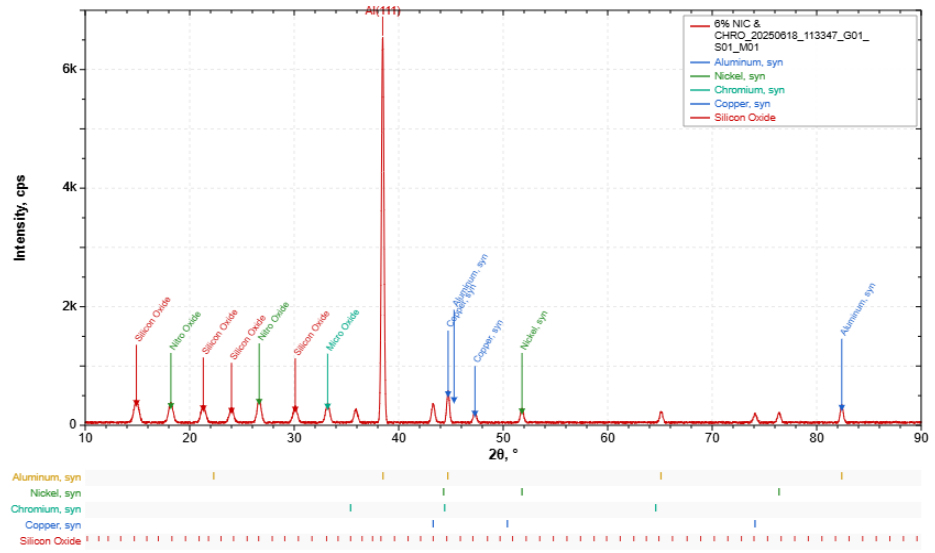

(d)

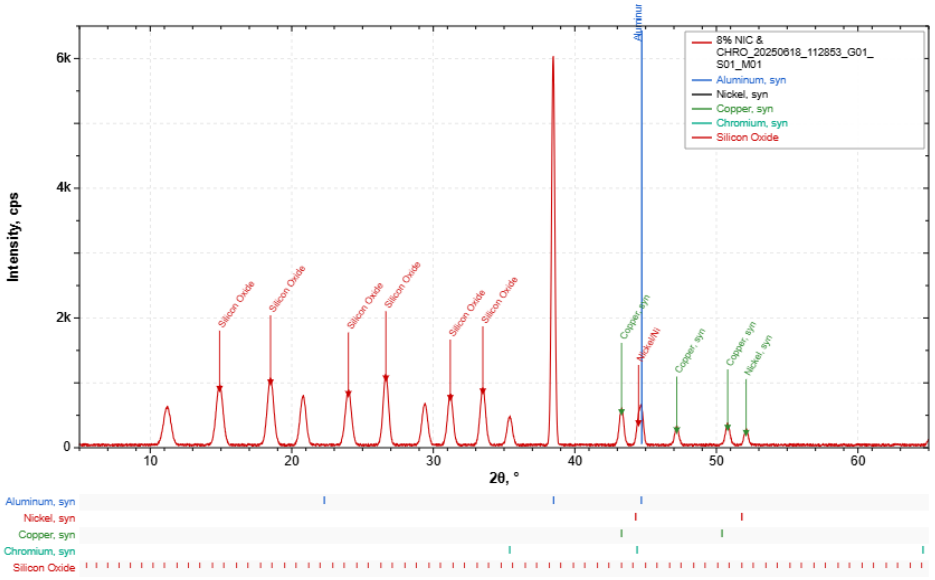

(e)

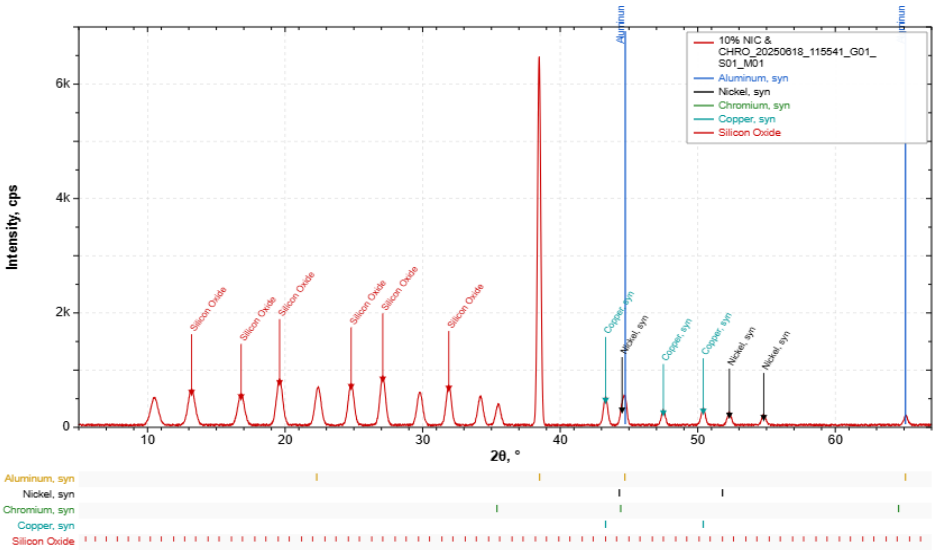

(f)

Figure 12. (a) Pure Al5Si3Cu (b) reinforced Al5Si3Cu with 2g of Ni-Cr (c) reinforced Al5Si3Cu with 4g of Ni-Cr, (d) reinforced Al5Si3Cu with 6g of Ni-Cr (e) reinforced Al5Si3Cu with 8g of Ni-Cr and (f) reinforced Al5Si3Cu with 10g of Ni-Cr.

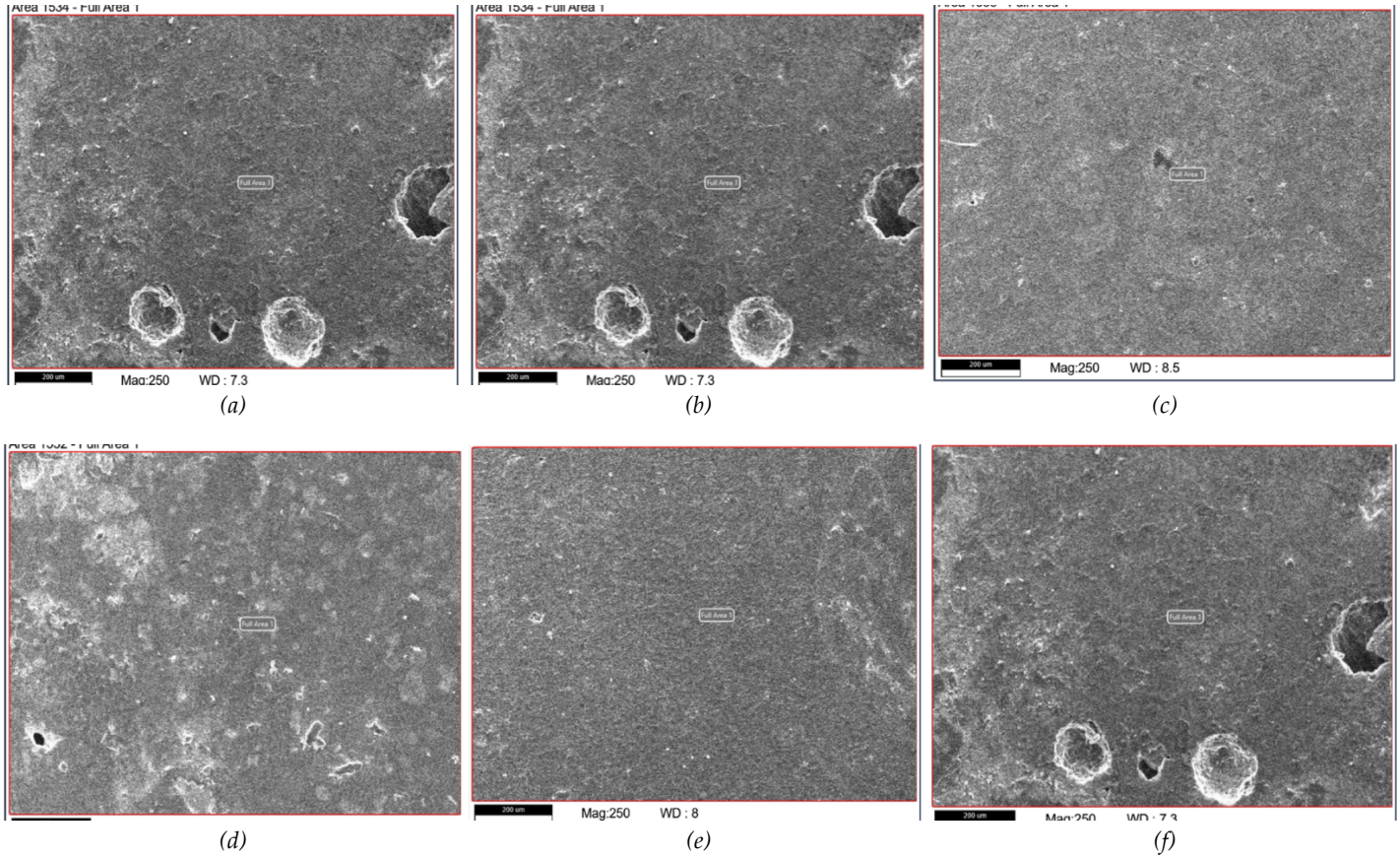

Figure 13. (a) Pure Al5Si3Cu (b) reinforced Al5Si3Cu with 2g of Ni-Cr (c) reinforced Al5Si3Cu with 4g of Ni-Cr, (d) reinforced Al5Si3Cu with 6g of Ni-Cr (e) reinforced Al5Si3Cu with 8g of Ni-Cr and (f) reinforced Al5Si3Cu with 10g of Ni-Cr.

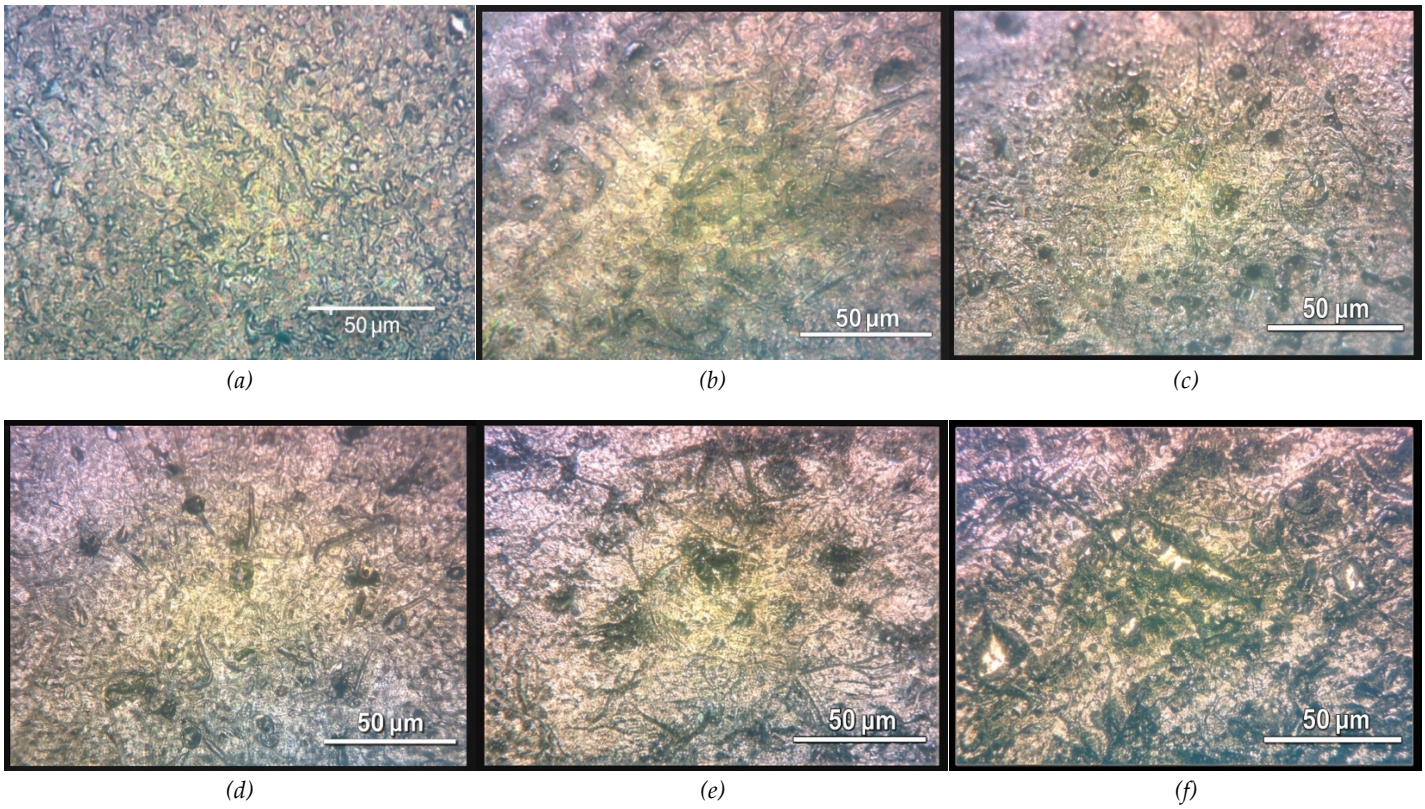

Figure 14. (a) Pure Al5Si3Cu (b) reinforced Al5Si3Cu with 2g of Ni-Cr (c) reinforced Al5Si3Cu with 4g of Ni-Cr, (d) reinforced Al5Si3Cu with 6g of Ni-Cr (e) reinforced Al5Si3Cu with 8g of Ni-Cr and (f) reinforced Al5Si3Cu with 10g of Ni-Cr.

Table 10. Summary of the SEM results of Al5Si3Cu-Ni-C.

Alloy Composition	Key Microstructural Features	Possible Microstructural Mechanism
Pure Al5Si3Cu	Homogeneous α-Al + Al_2Cu/Si	Solid solution strengthening
2 g Ni-Cr	Fine Ni-Cr dispersoids	Localized grain boundary pinning (limited effect)
4 g Ni-Cr	Clustered Ni-Cr phases	Dislocation interaction with clustered particles
6 g Ni-Cr	Uniform intermetallic network	Particle-matrix interaction
8 g Ni-Cr	Uniform intermetallic network	Restricted dislocation mobility
10 g Ni-Cr	Dense and clustered Ni-Cr	Intermetallic precipitation with agglomeration

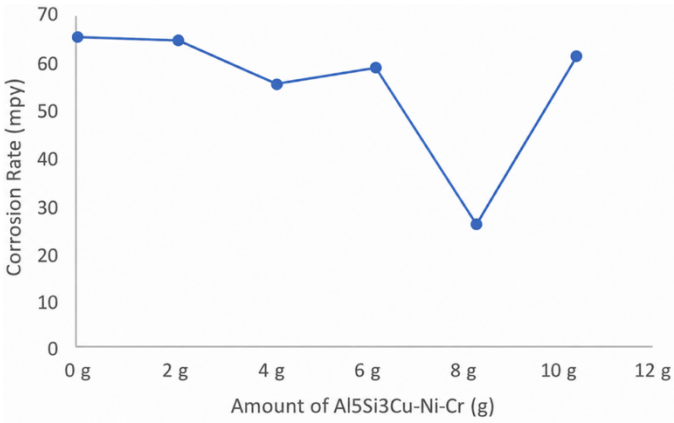

Figure 15. Corrosion level of reinforced Al5Si3Cu-Ni-Cr.

Table 11. Comparison of corrosion behaviour of reinforced Al5Si3Cu with Ni-Cr.

Amount of Ni-Cr in Al5Si3Cu	Icorr (μA)	Ecorr (V)	Corrosion Rate (mpy)
0g	144.0	-1.100	65.65
2g	143.0	-1.220	65.28
4g	122.0	-1.150	55.97
6g	130.0	-0.923	59.21
8g	53.10	-0.955	24.24
10g	135.0	-0.970	61.56

summarises the SEM results. The effect of Ni-Cr addition to Al5Si3Cu reduces its mechanical strength.

3.6. Optical Microstructure

The microstructure of the Al5Si3Cu alloy reinforced with varying percentages of Ni-Cr, as shown in the image, reveals that the alloy elements have a significant impact on the alloy. Figure 14b shows the microstructure of 2g Ni-Cr; however, there is no visible or noticeable difference when compared with the unreinforced Al5Si3Cu. The formation of compound Ni-Cr-rich compounds gives way to a relatively coarse and heterogeneous structure characterised by dendritic α-Al matrix regions and large, irregular intermetallic phases dispersed throughout the matrix, as shown in Figure 14b-f. In Figure 14f, bright white regions are indicative of Ni-rich and Cr-rich intermetallic compounds, likely consisting of Al_3Ni and Cr-based precipitates, which appear clustered and relatively large. The dark grey matrix represents the primary aluminium phase, while the interdendritic regions show a mixture of eutectic silicon and fragmented Cu-containing intermetallics. This microstructure suggests excessive intermetallic formation and possible phase segregation due to high Ni-Cr content. According to recent findings by [21], [31], [33], excessive Ni and Cr additions in aluminium alloys lead to the precipitation of large, brittle intermetallic particles along dendrite boundaries, which act as crack initiation points under mechanical loading. The observed coarsening in the microstructure can be attributed to insufficient undercooling and limited nucleation sites during solidification, allowing intermetallic compounds to grow unchecked, thereby reducing the toughness and ductility of the alloy. Furthermore, the high thermal conductivity difference between Ni, Cr intermetallics, and the Al matrix introduces localised cooling gradients during solidification. This promotes dendritic segregation and the formation of non-uniform microstructures, as supported by recent work in Al-Si-Cu-Ni alloys showing that excess Ni promotes thermal gradient-induced phase coarsening. Furthermore, the microstructural results indicate that Ni-Cr additions promote the formation of intermetallic phases within the Al5Si3Cu matrix. The influence of these phases on the overall mechanical response is likely related to their distribution, morphology, and interaction with the surrounding matrix. This leads to mechanical property deterioration, underscoring the need to optimise Ni-Cr additions (ideally near 2g - 4g) to achieve a fine, uniformly distributed microstructure that balances hardness with toughness for enhanced performance in wear-critical applications.

3.7. Corrosion Behaviour

From the results, the unreinforced Al5Si3Cu shows high corrosion activity (Icorr = 144 μA, corrosion rate = 65.65 mpy, Ecorr = –1.100 V), consistent with active dissolution in the test environment. The introduction of 2 g and 4g of Ni-Cr gave improved corrosion characteristics, indicating the formation of coating anodic reactions, a result that is similar to insufficient film formation to inhibit anodic reactions. Similar behaviour has been reported by [10], [34]. At 8g of Ni-Cr, the alloy corrosion behaviour became optimal with the corrosion level dropping to 24.24 mpy; corrosion current density (Icorr) also dropped to 53.10 μA, and corrosion potential (Ecorr) rose to a less negative –0.955 V, indicating reduced anodic dissolution and reinforced passivation. That is, a complete formation of a protective corrosion film. This drastic improvement in the corrosion behaviour at the introduction of 8g Ni-Cr conforms with studies of [35], [36] showing that optimal addition of these alloying elements fosters

the formation of a thick, adherent passive corrosion protective film comprising multiple layers of oxides, greatly enhancing corrosion resistance. This phenomenon is also in alignment with newly published research on microstructural refinement and passive-film thickening, increasing protection by [37], [38]. However, at a percentage of ≥ 10 g of Ni-Cr, the corrosion behaviour declined as seen from Table 11 and Figure 15. The change in the corrosion behaviour suggests that the alloy has become oversaturated with excess additives (Ni-Cr), thereby causing nucleate defects or metastable inclusions in the passive film, causing localised corrosion. Such behaviour was reported in a study conducted by [39] in 2024, with high additive content enhancing inhomogeneous passive film layers.

4. Conclusions

The comprehensive analysis, encompassing Brinell hardness, impact toughness, tensile strength, abrasive wear, compressive test, X-ray Diffraction (XRD), Scanning Electron Microscopy (SEM), microstructural examination, and corrosion behaviour, provided insights into how these additions significantly impacted the material's performance. The findings reveal that the mechanical properties were significantly impacted by the introduction of Ni-Cr in varying amounts, generally leading to a reduction in Brinell hardness, impact toughness, compressive strength, and tensile strength when compared to the unalloyed Al5Si3Cu. These microstructural changes, observed through SEM and XRD, explain the observed deterioration in the material's ability to withstand deformation, absorb energy, and resist tensile forces. Conversely, the abrasive wear performance exhibited a different response to Ni-Cr additions. An optimal concentration of 2 g Ni-Cr significantly improved the alloy's wear resistance, achieving the lowest wear rate and highest wear resistance among all compositions.

The machining performance of both unreinforced and reinforced Al5Si3Cu with Ni-Cr alloys shows a direct relationship between increased Ni-Cr content and higher cutting forces and surface roughness, particularly at lower spindle speeds. These findings emphasise the importance of optimising both material composition and cutting parameters to enhance machinability in Ni-Cr–reinforced aluminium alloys. This microstructural evolution directly correlated with the observed mechanical behaviour, emphasising that controlling the distribution and size of these intermetallic phases is paramount for optimising the alloy's performance.

In terms of corrosion behaviour, the study revealed a significant impact of Ni-Cr additions. While the unreinforced Al5Si3Cu exhibited high corrosion activity, an optimal concentration of 8g Ni-Cr drastically improved corrosion resistance, leading to a substantial drop in corrosion rate and current density. This indicates that there is an optimal range for Ni-Cr additions to achieve enhanced corrosion protection without compromising the film's integrity. Further study should be carried out with more material, equipment, heat treatment and other forms of processing, such as proper stir casting and powder metallurgy (PM).

5. Declarations

5.1. Author Contributions

Omogbolade L. Adepitan: Methodology, Validation, Formal analysis, Investigation, Resources, Formal analysis, Investigation, Resources, Data Curation, Writing - Original Draft, Writing - Review & Editing, Visualization, Supervision, Project administration, Funding acquisition; **Olusegun Olufemi Ajide:** Conceptualization, Methodology, Validation, Formal analysis, Investigation, Resources, Writing - Review & Editing, Visualization, Supervision, Project administration, Funding acquisition.

5.2. Institutional Review Board Statement

Not applicable.

5.3. Informed Consent Statement

Not applicable.

5.4. Data Availability Statement

The data presented in this study are available on request from the corresponding author.

5.5. Acknowledgment

Not applicable.

5.6. Conflicts of Interest

The authors declare no conflict of interest.

6. References

[1] N. Divakaran, P. D. Jyoti, P. V. Ajay Kumar, M. Smita, R. Ananthakumar, and K. N. Sanjay, "Comprehensive review on various additive manufacturing techniques and its implementation in electronic devices," *J. Manuf. Syst.*, vol. 62, pp. 477–502, 2022. https://doi.org/10.1016/j.jmsy.2022.01.002.

[2] N. E. Udoye, F. S. Oluwatowo, "The study on electrical and mechanical impact of snail shell reinforced AA6061 matrix composites," *Am. J. Chem. Eng.*, vol. 11, no. 4, 2023. https://doi.org/10.11648/j.ajche.20231104.12.

[3] Q. Zheng, J. Wang, H. Jiang, L. Zhang, J. Zhou, and J. He, "Effect of micro-alloying element La on corrosion behavior of Al-Mg-Si alloys," *Corros. Sci.*, vol. 179, Art. no. 109113, 2020. https://doi.org/10.1016/j.corsci.2020.109113.

[4] M. S. Remøe, K. Marthinsen, I. Westermann, K. Pedersen, J. Røyset, and C. Marioara, "The effect of alloying elements on the ductility of Al-Mg-Si alloys," *Mater. Sci. Eng. A*, vol. 693, pp. 60–72, 2017. https://doi.org/10.1016/j.msea.2017.03.078.

[5] J. Zhao *et al*, "The effect of Mn content on a novel Al–Mg–Si-Sc-Zr alloy produced by laser powder bed fusion: The microstructure and mechanical behavior," *J. Mater. Res. Technol.*, vol. 28, pp. 989–1001, 2023. https://doi.org/10.1016/j.jmrt.2023.11.048.

[6] O. O. Ajide, O. C. Adedokun, N. Idusuyi, N. Kumar, O. A. Aogo, A. S. Ajao, K. K. Adebayo, A. Joshi, and C. Prakash, "Examining the mechanical response and microstructural evolution of heat-treated Al-5Si-3Cu alloy for automotive applications," *Adv. Mater. Process. Technol.*, 2023. https://doi.org/10.1080/2374068X.2023.2184602.

[7] Y. Liu, S. Ma, M. Gao, S. Peng, Y. Feng, and R. Guo, "Enhanced comprehensive performance via alloying and rheo-diecasting in a semi-solid Al–Si–Fe–Mg–Cu–Sr alloy," *J. Mater. Res. Technol.*, vol. 25, pp. 420–439, 2023. https://doi.org/10.1016/j.jmrt.2023.05.222.

[8] F. Sun, X. Wen, S. Sun, Y. Lu, W. Xiao, and C. Ma, "Effects of Cr addition on the microstructure and mechanical properties of an Al–Si–Cu–Mg alloy," *Materials*, vol. 17, no. 14, Art. no. 3607, 2024. https://doi.org/10.3390/ma17143607.

[9] S. Singh, D. Prathap, D. Ananthapadmanaban, D. Elil Raja, T. Sonar, M. Ivanov, P. Prabhuraj, and V. Sivamaran, "Investigating the microstructure, tensile strength, and acidic corrosion behaviour of liquid metal stir casted aluminium-silicon carbide composite," *Adv. Mater. Sci. Eng.*, pp. 1–11, 2023. https://doi.org/10.1155/2023/2131077.

[10] L. Xiao *et al.*, "Microstructure and mechanical properties of cast Al-Si-Cu-Mg-Ni-Cr alloys: Effects of time and temperature on two-stage solution treatment and ageing," *Materials*, vol. 16, no. 7, Art. no. 2675, 2023. https://doi.org/10.3390/ma16072675.

[11] S. Al-Alimi *et al.*, "Recycling aluminium for sustainable development: A review of different processing technologies in green manufacturing," *Results Eng.*, vol. 23, Art. no. 102566, 2024. https://doi.org/10.1016/j.rineng.2024.102566.

[12] M. Y. Khalid, R. Umer, and K. A. Khan, "Review of recent trends and developments in aluminium 7075 alloy and its metal matrix composites (MMCs) for aircraft applications," *Results Eng.*, vol. 20, Art. no. 101372, 2023. https://doi.org/10.1016/j.rineng.2023.101372.

[13] A. Sánchez-Roncero, Ò. Garibo-I-Orts, J. A. Conejero, H. Eivazi, F. Mallor, E. Rosenberg, F. Fuso-Nerini, J. García-Martínez, R. Vinuesa, and S. Hoyas, "The Sustainable Development Goals and Aerospace Engineering: A critical note through Artificial Intelligence," *Results Eng.*, vol. 17, Art. no. 100940, 2023. https://doi.org/10.1016/j.rineng.2023.100940.

[14] A. Mehri, A. Abdollah-Zadeh, S. Entesari, T. Saeid, and J. T. Wang, "The effects of friction stir welding on microstructure and formability of 7075-T6 sheet," *Results Eng.*, vol. 18, Art. no. 101041, 2023. https://doi.org/10.1016/j.rineng.2023.101041.

[15] F. Haghdadi, R. Jamaati, and S. J. Hosseinipour, "Evading the strength-ductility trade-off dilemma in AA2024 alloy by short-term natural re-aging after T351 temper," *Heliyon*, vol. 10, no. 5, Art. no. e27257, 2024. https://doi.org/10.1016/j.heliyon.2024.e27257.

[16] O. Asghar, M. Franceschi, P. Ferro, and F. Bonollo, "A novel aluminium alloys design strategy for low usage of critical raw materials and high casting processibility for automotive applications," *Int. J. Metalcast.*, 2025. https://doi.org/10.1007/s40962-024-01502-6.

[17] H. Zhu, C. Xia, H. Zhang, D. Zhao, M. Wang, and H. Wang, "Design of non-heat treatable high pressure die casting Al alloys: A review," *J. Mater. Eng. Perform.*, vol. 33, no. 17, pp. 8601–8626, 2024. https://doi.org/10.1007/s11665-024-09477-5.

[18] H. F. Amin, A. I. Khwakaram, O. S. Mahmood, P. M. Karim, and R. R. Amin, "Effect of vegetable oil quenchants and precipitation hardening on the mechanical properties of aluminium alloy (AA2024)," *J. Eng.*, vol. 30, no. 8, pp. 85–100, 2024. https://doi.org/10.31026/j.eng.2024.08.06.

[19] W. Rativa-Parada and S. Nilufar, "Influence of heat treatment on microstructure, mechanical properties, and damping behaviour of 2024 aluminium matrix composites reinforced by carbon nanoparticles," *Nanomaterials*, vol. 14, no. 16, Art. no. 1342, 2024. https://doi.org/10.3390/nano14161342.

[20] R. M. El-Shorbagy, Z. M. El-Baradie, and A. I. Abdel-Aziz, "Microstructure and mechanical properties of 2024 aluminium alloy with and without rare-earth and thermomechanical treatment after multi-pass stir friction processing," *Int. J. Metalcast.*, vol. 18, pp. 2508–2524, 2024. https://doi.org/10.1007/s40962-023-01191-7.

[21] Z. Xie, L. Zhou, J. Li, Y. Duan, M. Peng, H. Xiao, X. Du, Y. Zhao, and M. Li, "Mechanical and corrosion properties of AA2024 aluminium alloy with multimodal gradient structures," *Metals*, vol. 15, no. 2, p. 177, 2025. https://doi.org/10.3390/met15020177.

[22] M. Vončina, T. Balaško, M. Petrič, J. Medved, O. Modrijan, and J. Li, "Effect of the addition of Ni and Cu on solidification microstructure evolution of Al-5Si-0.5Mg alloys," *Int. J. Metalcast.*, 2025. https://doi.org/10.1007/s40962-024-01449-8.

[23] M. Naseri, A. O. Moghaddam, N. Shaburova, D. Mikhailov, D. Gholami, A. I. Mourad, A. Pellinen, and E. Trofimov, "Upgrading the strength-ductility trade-off and wear resistance of Al0.25CoCrFeNiCu and Al0.45CoCrFeNiSi0.45 high-entropy alloys through severe cold rolling process," *Mater. Today Commun.*, vol. 38, p. 108036, 2024. https://doi.org/10.1016/j.mtcomm.2024.108036.

[24] M. H. Abdelaziz, H. W. Doty, S. Valtierra, and F. H. Samuel, "Mechanical performance of Zr-containing 354-type Al–Si–Cu–Mg cast alloy: Role of additions and heat treatment," *Adv. Mater. Sci. Eng.*, vol. 2018, p. 5715819, 2018. https://doi.org/10.1155/2018/5715819.

[25] A. S. J. Al-Zubaydi, N. Gao, S. Wang, and P. A. S. Reed, "Microstructural and hardness evolution of additively manufactured Al–Si–Cu alloy processed by high-pressure torsion," *J. Mater. Sci.*, vol. 57, no. 19, pp. 8956–8977, 2022. https://doi.org/10.1007/s10853-022-07234-4.

[26] E. Kocaman, "Effect of Al5Ti1B and Al8B on the microstructure, wear and corrosion behavior of CuZn19Al6 bronze alloy," *Mater. Today Commun.*, vol. 36, p. 106551, 2023. https://doi.org/10.1016/j.mtcomm.2023.106551.

[27] H. Mindivan, M. Baydogan, E. S. Kayali, and H. Cimenoglu, "Wear behaviour of 7039 aluminum alloy," *Mater. Charact.*, vol. 54, no. 3, pp. 263–269, 2005. https://doi.org/10.1016/j.matchar.2004.12.004.

[28] B. Zhao, Y. Wang, J. Peng, X. Wang, W. Ding, X. Lei, B. Wu, M. Zhang, J. Xu, L. Zhang, and R. Das, "Overcoming challenges: Advancements in cutting techniques for high strength-toughness alloys in aero engines," *Int. J. Extreme Manuf.*, 2024. https://doi.org/10.1088/2631-7990/ad8117.

[29] L. Cao, Y. Liu, H. Chen, L. Zhang, H. Sun, and G. Bi, "Investigation of intermetallics formation and joint performance of laser welded Ni to Al," *Appl. Sci.*, vol. 13, no. 3, p. 1356, 2023. https://doi.org/10.3390/app13031356.

[30] X. Meng, W. Zhang, Y. Ma, Q. Xiang, Y. Ren, and K. Qiu, "Improvements on the mechanical properties of Al 6063 alloy by microalloying with Cu and Cr elements," *Int. J. Metalcast.*, vol. 18, pp. 1309–1317, 2024. https://doi.org/10.1007/s40962-023-01110-w.

[31] S.-S. Li, X. Yue, Q. Li, H. Peng, B. Dong, T. Liu, H. Yang, J. Fan, S. Shu, F. Qiu, and Q. Jiang, "Development and applications of aluminum alloys for aerospace industry," *J. Mater. Res. Technol.*, vol. 27, pp. 944–983, 2023. https://doi.org/10.1016/j.jmrt.2023.09.274.

[32] A. Thakur, A. Kumar, S. Kaya, R. Marzouki, F. Zhang, and L. Guo, "Recent advancements in surface modification, characterization and functionalization for enhancing the biocompatibility and corrosion resistance of biomedical implants," *Coatings*, vol. 12, no. 10, p. 1459, 2022. https://doi.org/10.3390/coatings12101459.

[33] Z. Lei, S. Wen, H. Huang, W. Wei, and Z. Nie, "Grain refinement of aluminium and aluminium alloys by Sc and Zr," *Metals*, vol. 13, no. 4, p. 751, 2023. https://doi.org/10.3390/met13040751.

[34] D. Tsotetsi, L. Noto, D. Idisi, E. Benecha, M. Dhlamini, and P. Mbule, "Computational and experimental investigation of the structure, morphology, optical and electrical properties of TiO_2 and caffeine adsorbed TiO_2 in methyl ammonium lead iodide," *Mater. Today Commun.*, vol. 38, p. 108453, 2024. https://doi.org/10.1016/j.mtcomm.2024.108453.

[35] M. A. Ahmed, S. Amin, and A. A. Mohamed, "Current and emerging trends of inorganic, organic and eco-friendly corrosion inhibitors," *RSC Adv.*, vol. 14, no. 43, pp. 31877–31920, 2024. https://doi.org/10.1039/D4RA05662K.

[36] E. Kocaman and S. Şirin, "Effect of Al5Ti1B grain refiner and Al10Sr modifier on mechanical properties and corrosion behavior of A360 alloy," *Int. J. Automot. Sci. Technol.*, vol. 7, no. 1, pp. 30–36, 2023. https://doi.org/10.30939/ijastech..1237345.

[37] M. Liu *et al*., "Corrosion and passive film characteristics of 3D printed NiTi shape memory alloys in artificial saliva," *Rare Metals*, vol. 42, no. 9, pp. 3114–3129, 2023. https://doi.org/10.1007/s12598-023-02329-6.

[38] P. Moazzen *et al*., "Optimum corrosion performance using microstructure design and additive manufacturing process control," *npj Mater. Degrad.*, vol. 9, p. 10, 2025. https://doi.org/10.1038/s41529-024-00548-5.

[39] S. B. Inman, M. A. Wischhusen, J. Qi, S. J. Poon, S. R. Agnew, and J. R. Scully, "Variation of the passive film on compositionally concentrated dual-phase $Al_{0.3}Cr_{0.5}Fe_2Mn_{0.25}Mo_{0.15}Ni_{1.5}Ti_{0.3}$ and implications for corrosion," *Metall. Mater. Trans. A*, vol. 55, no. 12, pp. 4776–4795, 2024. https://doi.org/10.1007/s11661-024-07572-9.